(74)

# Thermohaline Circulation Stability in a Coupled Land-Ocean-Atmosphere Box Model

by

DAVID MICHAEL SIRKIN

S.M. (Management) 1992, Massachusetts Institute of Technology

B.A.S. (C.S.E.) 1985, University of Pennsylvania

Submitted to the Department of Earth, Atmospheric and Planetary Science
in partial fulfillment of the requirements for the degree of

MASTER OF SCIENCE IN GEOSYSTEMS

at the

MASSACHUSETTS INSTITUTE OF TECHNOLOGY

September, 1998



Author _____
Department of Earth, Atmospheric and Planetary Science
June 26, 1998

Certified by _____
Jochem Marotzke, Associate Professor
Department of Earth, Atmospheric and Planetary Science
Thesis Supervisor

Accepted by _____
Thomas Jordan, Professor of Geophysics
Department of Earth, Atmospheric and Planetary Science
Department Head

# Thermohaline Circulation Stability in a Coupled Land-Ocean-Atmosphere Box Model

by

DAVID MICHAEL SIRKIN

Submitted to the Department of Earth, Atmospheric and Planetary Science
in partial fulfillment of the requirements for the degree of

MASTER OF SCIENCE IN GEOSYSTEMS

ABSTRACT

Global climate reflects a complex interaction among the continents, the oceans and the atmosphere. Exactly how these interactions occur remains one of the great questions about the Earth system. To address this issue, a simple box model representing one hemisphere with land, ocean and atmosphere components is developed and analyzed. The specific question addressed is how the inclusion of separate temperatures over land and the ocean affects the existence and stability of meridional ocean flow equilibria. Temperature and salinity differences are the main determinants of the strength and direction of ocean flow. Both heat and moisture fluxes are determined from the global mean meridional temperature gradient. As temperatures over land are increasingly allowed to deviate from those over the ocean, the gradient over land becomes larger and has more influence over the mean. The stability of the ocean's poleward flow equilibrium is then more sensitive to over-estimation of the size of the ocean basin or atmospheric heat and moisture transports. Its flow is also weaker than before, due to smaller temperature gradient. An equatorward flow equilibrium with no oceanic meridional temperature contrast is then possible.

Thesis Supervisor: Jochem Marotzke, Associate Professor
Department of Earth, Atmospheric and Planetary Science

# Table of Contents

# List of Figures



# List of Tables

# 1 Introduction

## 1.1 The Thermohaline Circulation

The oceans and atmosphere form a global-scale system that determines climate patterns over large regions. Broadly, the ocean's role is through the storage and transport of heat. Due to Earth's shape and orbit, polar and equatorial oceans are heated at different rates. The amount of heat stored and released by each depends on its density and volume. Density varies with depth, temperature and salinity, while volume depends on basin size. In effect, low- and high-latitude, shallow and deep oceans respond differently to changing conditions.

The uneven heating of polar and equatorial basins creates a meridional (north-south) temperature-driven density gradient. The resulting tendency is characterized by (1) deep equatorward flows of polar water to warmer, less dense regions and (2) near-surface poleward flows of the warmed water toward its origin. At the sea surface where the ocean and atmosphere interact, the same uneven heating leads to net evaporation from low latitudes and precipitation into high latitudes. The freshwater transport therefore creates a meridional salinity-driven gradient. The resulting tendency counteracts the temperature-driven state, with (1) deep poleward flows of salty equatorial water to colder but less dense regions and (2) near-surface equatorward flows of the fresher polar water toward its origin. The competing effects result in a global thermohaline circulation (THC).

The continents interact with the ocean-atmosphere system through their own heat and moisture transport mechanisms. Temperatures over land are governed by radiative heating and the ocean's influence. Some of the freshwater from the ocean's evaporation-precipitation cycle is captured

and diverted meridionally as well as zonally (east-west) by river flow. Depending on the strength and direction of these flows, the land's influence may balance or reinforce the THC feedbacks.

Observations show that ocean circulation is in fact initialized by deep cold water formation in the North Atlantic. From there, water moves toward the equator and into the Pacific and Indian oceans, where it is warmed, upwells, and returns near the surface (Gordon, 1986). As a result, heat is transported primarily from warm to cold regions. However, in the South Atlantic, heat is transported northward toward warm regions. Other equilibrium flow states for vertical and horizontal transport of water are theoretically possible, and paleoclimatic observations (Boyle, 1990; Broecker et al., 1995) indicate that circulation strength and pattern have varied through time. Two relevant questions for modelers are then (1) how stable is the current global THC pattern and (2) what are the feedbacks that lead to one scenario or another?

## 1.2 Modeling Approaches

Both general circulation models (GCMs) and simple box models (SBMs) have been used to study the THC. GCMs formulate the equations of motion through finite difference methods while SBMs use a limited number of parameterized equations. Perhaps because of computational differences, GCMs are used mostly to reproduce current or past climate; simple models are used mostly as a heuristic tool to guide later GCM studies.

Oceanic GCMs include temperature and salinity effects, and formulate the equations of motion through finite difference methods (Bryan, 1986; Marotzke and Willebrand, 1991). Atmospheric feedbacks are generally not included explicitly, but are implied through the surface boundary conditions. Coupled GCMs (Manabe and Stouffer, 1988) remedy this by introducing ocean-atmosphere interaction through the exchange of heat, water and momentum and can include land components. These models benefit from representative geography and include seasonal variations in insolation and humidity-dependent cloud cover.

Stommel (1961) identified the competing temperature and salinity fields as the fundamental cause of multiple equilibria in his model. Twenty-five years later, Bryan (1986) was the first oceanic GCM with freely evolving surface salinity. Its solutions were also characterized by multiple

equilibria for upwelling and overturning. However, the work did not explore the effects of asymmetric surface forcing, basin geometry or changing evaporative fluxes. Marotzke and Willebrand's (1991) model comprised two ocean basins connected by a circumpolar channel. Circulation was driven by wind forcing, restorative tendencies in sea-surface temperature, and freshwater fluxes in the surface salinity budget. Using the same set of boundary conditions, four equilibria were found, where one solution corresponded to today's global circulation pattern.

The simple model approach to the ocean-atmosphere system provides similar system insights and intuitive analysis while requiring less computational complexity. Marotzke's (1996) four-box ocean-atmosphere model includes only one hemisphere and averages atmospheric transports, but results in complex feedback behavior. Like the coupled GCMs, the primary feedback loops are (1) the ocean's tendency to eliminate gradients through mean flow and mixing, (2) oceanic heat and salinity transports, and (3) atmospheric heat and moisture transports. Also like the larger models, temperature- and salinity-dominated steady solutions are possible. But while the idealized global GCMs produce at most four equilibria, the simple box models configured globally can result in as many as sixteen (Marotzke and Willebrand, 1991). The difference may be due to the exclusion of a southern ocean connection between Atlantic and Pacific Oceans, or parameterizations for atmospheric forcing or surface heat and moisture fluxes.

The parameterization the coupled box models is based in part on having thoroughly mixed ocean basins and atmosphere boxes (Marotzke and Stone, 1995, Marotzke, 1996). Temperatures above the ocean are therefore determined by the sea-surface temperature. Temperatures above the land equal those above the ocean at the same latitude. Therefore, all surface temperatures are prescribed by the ocean, no matter how small (as long as it exists). Configured like this, a model may not capture the dynamics that we see along coastlines. For example, there are differences in land and ocean heat storage capacities, varying efficiencies in near-shore eddy exchange, and seasonal variations in ocean-land temperature gradients. We can ask if this is a reasonable outcome and what would happen if the uniformity in zonal atmospheric temperatures no longer held. Marotzke (1996) describes a simple formulation for incorporating separate temperatures over land into a four-box model. The equations are not solved analytically or numerically for steady-states and the feedback analysis only considers the case with complete zonal mixing. The question

addressed here is whether allowing finite zonal heat transport efficiency changes the equilibrium solutions or the feedback stucture or strength. If the change is significant, then the size of the continents and the atmospheric temperatures above them may have a strong influence on global temperatures and the existing THC regime. If the change is not so significant, the ocean would still have the strongest influence on global climate and the assumption of atmospheric uniformity would not be too unrealistic.

## 1.3 Thesis Organization

Section 2 following the introduction develops the model's framework. The equations for conservation of heat and moisture are combined with those governing zonal and meridional fluxes. Assuming a linear atmosphere, analytical solutions are found. Section 3 explores the equilibrium solutions. Parameters' effects on the geometry of solutions are used as references to compare with the model under zonally uniform and stratified atmospheres. The feedbacks that lead to different solutions are presented, followed by a numerical stability analysis of the temperature-dominated steady-state. Section 4 summarizes results and suggests ways the model can be further developed. Following the References, two Appendices include (A) derivations of steady-state equations and (B) program diagrams and code.

# 2 Model Description

The model's construction is based on Marotzke (1996) sections 2 (Model Formulation) and 4 (Land Effects). The description of equations closely follows the one therein.

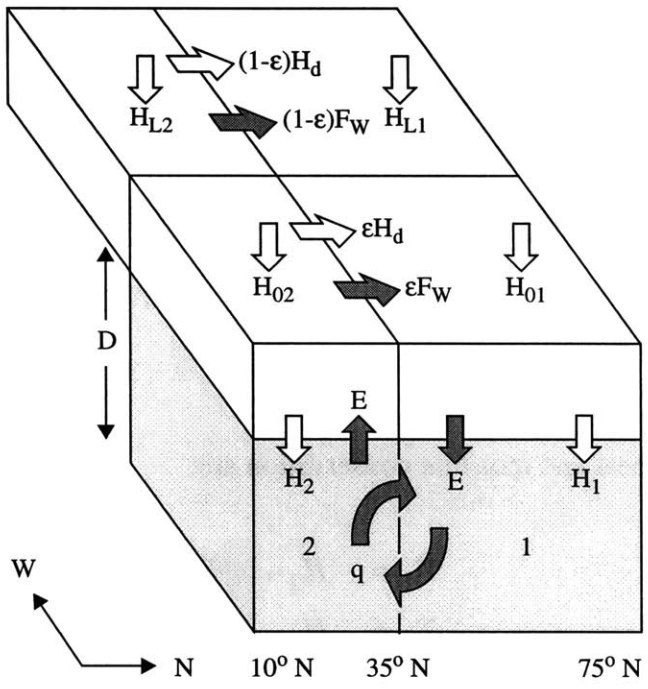


**Figure 1:** Vertical view of the box model in the northern hemisphere facing west. The ocean and the atmosphere over it are in the foreground; the atmosphere over land is in the background. Heat fluxes are represented by light arrows and moisture fluxes by dark arrows. Northward atmospheric transports are split ε over the ocean and (1-ε) over land.

## 2.1 Basic Equations

The system is represented as six boxes: two oceanic and four atmospheric (figure 1). The two ocean boxes represent high-latitude and low-latitude basins (numbered 1 and 2, respectively) of

depth $D$ that are completely mixed in both temperature and salinity. At the surface, $H_1$ and $H_2$ are heat gain into each box; $E$ is net evaporation from low-latitudes and net precipitation into high-latitudes. $q$ is the flow strength between boxes. It is positive when water moves poleward near the surface. The four remaining boxes represent the atmosphere above high-latitude and low-latitude ocean and land. The atmosphere's vertical structure is assumed fixed, so that surface air temperatures equal the sea-surface temperatures below. At the top, $H_{01}$ and $H_{02}$ are heat gain over the ocean; $H_{L1}$ and $H_{L2}$ are heat gain over land. $H_d$ is the meridional energy transport, split $\varepsilon H_d$ over the ocean and $(1 - \varepsilon)H_d$ over land. $F_W$ is the meridional moisture transport, also split $\varepsilon F_W$ over the ocean and $(1-\varepsilon)F_W$ over land. $\varepsilon$ used this way defines the ocean area relative to the total surface area.

A key assumption behind the model is center manifold theory, which states that atmospheric heat and moisture equilibration timescales (about a month and a week, respectively) are sufficiently shorter than the ocean's (several hundred years) to be assumed virtually in equilibrium. Heat storage and transport are based on meridional gradients, which are controlled by the ocean. We therefore begin by defining ocean temperature and salinity gradients:

$$T \equiv T_2 - T_1 \tag{1}$$

$$S \equiv S_2 - S_1 \tag{2}$$

Then the equations for heat and moisture conservation are:

$$\dot{T}_1 = H_1 - |q|T \tag{3}$$

$$\dot{T}_2 = H_2 - |q|T \tag{4}$$

$$\dot{S}_1 = -H_S + |q|S \tag{5}$$

$$\dot{S}_2 = H_S - |q|S \tag{6}$$

To convert ocean surface heat gains $H_1$ and $H_2$ into fluxes $\tilde{H}_1$ and $\tilde{H}_2$, multiply each by the heat capacity of a unit column of water:

$$c\rho_0 D \cong 2\times10^{10}\ Jm^{-2}K^{-1} \tag{7}$$

Flow strength $q$ is a linear function of the meridional density gradient:

$$q = k(\rho_1 - \rho_2) = k(\alpha T - \beta S) \tag{8}$$

where $\alpha$ and $\beta$ are thermal and haline expansion coefficients. The hydraulic constant $k$ represents the dynamics between density and the flow field. The surface salinity flux $H_S$ is a linear function of the surface freshwater flux:

$$H_S = S_0 \frac{E}{D} \tag{9}$$

where $S_0$ is a reference salinity.

For the atmosphere, we assume heat and moisture capacities are negligible. By parameterizing energy gain at the top and horizontal heat and moisture fluxes within, atmosphere-ocean exchanges are determined as residuals of the steady-state budgets. We can now define the land temperature gradient as:

$$T_L \equiv T_{L2} - T_{L1} \tag{10}$$

Radiation terms for the top of the atmosphere are linear functions of the surface temperature below:

$$H_{01} = A_1 - BT_1 \tag{11a}$$
$$H_{02} = A_2 - BT_2 \tag{11b}$$
$$H_{L1} = A_1 - BT_{L1} \tag{12a}$$
$$H_{L2} = A_2 - BT_{L2} \tag{12b}$$

where $A_1$ and $A_2$ are high-latitude (negative) and low-latitude (positive) shortwave radiation for 0 $^{o}$C surface temperature. $BT_1$, $BT_2$ (over the ocean) and $BT_{L1}$, $BT_{L2}$ (over land) then represent the longwave radiation components due to non-zero surface temperatures. Meridional heat and moisture transports $H_d$ and $F_W$ are evenly distributed around a latitude circle so $\varepsilon$ occurs over the ocean and (1-$\varepsilon$) over land:

$$H_d = \tilde{\chi}_n [T]^n \quad \text{for } n \geq 0 \tag{13}$$

$$F_W = \tilde{\gamma}_m [T]^m \quad \text{for } m \geq 0 \tag{14}$$

where the zonal mean temperature gradient is defined as:

$$[T] \equiv \varepsilon T + (1 - \varepsilon) T_L \tag{15}$$

The powers $n$ and $m$ and coefficients $\tilde{\chi}_n$ and $\tilde{\gamma}_m$ define alternative models that relate the transports to the temperature gradient. The remainder of the model description will use $n = m = 1$, so $\tilde{\chi} = \tilde{\chi}_1$ and $\tilde{\gamma} = \tilde{\gamma}_1$. Heat transport pairs $H_{OL1}$, $H_{OL2}$ and $H_{LO1}$, $H_{LO2}$ respectively cross the ocean-land and land-ocean boundaries and are periodic (figure 2). Only their zonal differences are used:

$$H_{OL1} - H_{LO1} = \mu (T_1 - T_{L1}) \tag{16a}$$

$$H_{OL2} - H_{LO2} = \mu (T_2 - T_{L2}) \tag{16b}$$

where $\mu$ is the atmospheric zonal heat mixing efficiency. No atmospheric zonal moisture mixing efficiency is explicitly prescribed. However, zonal heat transport is a factor in determining the zonal mean temperature gradient, which governs both meridional heat and moisture transports. Very efficient mixing produces a zonally uniform atmosphere where the temperatures over land equal those over the ocean at the same latitude and therefore have no distinct role in determining the meridional temperature gradient. Very inefficient mixing uncouples the temperatures—and therefore heat and moisture transports—over the land and ocean. Temperatures and gradients over the land can then independently influence the global mean meridional gradient.

## 2.2 Surface Meridional Fluxes

***Heat Over the Ocean and Land***

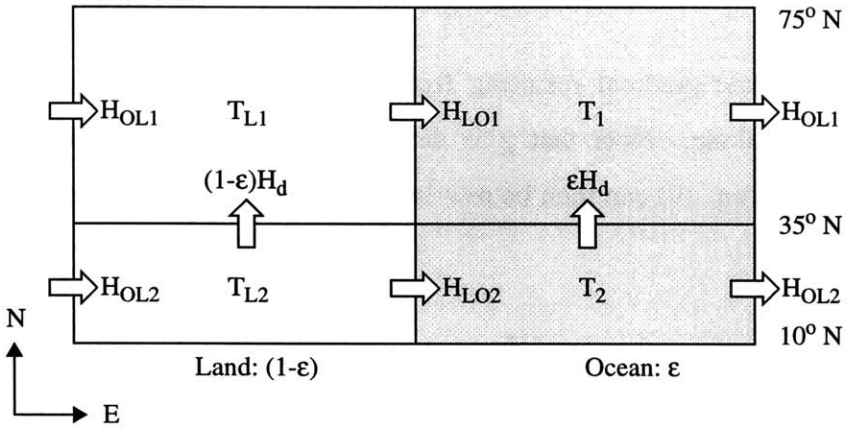


**Figure 2**: Overhead view of atmospheric heat transports. Meridional transport is split ε over the ocean and (1-ε) over land. Zonal transports have periodic boundaries and only their differences are used.

The atmospheric heat budgets over the ocean are functions of (1) energy gain at the top of the atmosphere, (2) heat gain at the ocean surface, (3) meridional heat flux between ocean boxes, and (4) zonal heat flux across the ocean-land boundary:

$$H_{01} - \tilde{H}_1 + H_d - \frac{\mu}{\varepsilon}(T_1 - T_{L1}) = 0 \tag{17}$$

$$H_{02} - \tilde{H}_2 - H_d - \frac{\mu}{\varepsilon}(T_2 - T_{L2}) = 0 \tag{18}$$

The differential surface heat flux, defined as:

$$\tilde{H}_T \equiv \tilde{H}_2 - \tilde{H}_1 \tag{19}$$

is then derived from these two equations:

$$\tilde{H}_T = (2\chi + B)\frac{B + \dfrac{\mu}{\varepsilon(1-\varepsilon)}}{B + 2\chi(1-\varepsilon) + \dfrac{\mu}{(1-\varepsilon)}}(T_E - T) \tag{20}$$

where the atmospheric equilibrium temperature gradient is defined as:

$$T_E \equiv T|_{q=0} = \frac{A_2 - A_1}{2\chi + B} \tag{21}$$

This is the steady-state gradient resulting from a balance between atmospheric dynamic and radiative transports alone. Note that $\chi$ is defined as $\tilde{\chi}$ divided by the total box area. The differential heat flux (eq. 19) can then be rewritten as a Newtonian (power) cooling law for ocean temperature:

$$\tilde{H}_T = \lambda_L (T_E - T) \tag{22}$$

where the Newtonian damping coefficient $\lambda_L$ is defined as:

$$\lambda_L \equiv \frac{1}{\varepsilon_L}\left(\frac{2\chi + B}{c\rho_0 D}\right) \tag{23}$$

and the effective ocean area ratio $\varepsilon_L$ is defined as:

$$\varepsilon_L \equiv \frac{B + 2\chi(1-\varepsilon) + \dfrac{\mu}{(1-\varepsilon)}}{B + \dfrac{\mu}{\varepsilon(1-\varepsilon)}} \tag{24}$$

$\lambda_L$ then relates the differential surface heat flux to ocean temperature differences. The prognostic equation for the meridional temperature difference (combine eqs. 3, 4 and 8 with 19 and 22) is:

$$\dot{T} = H_T - 2|q|T = \lambda_L (T_E - T) - 2k|\alpha T - \beta S|T \tag{25}$$

In steady-state:

$$(T_E - T) = \frac{2|q|T}{\lambda_L} \tag{26}$$

When there is no flow, $T_E = T$; when the flow is non-zero, $T_E > T$. An ocean that transports heat therefore reduces the meridional temperature gradient below what atmospheric transports alone would prescribe. The difference varies inversely with the strength of $\lambda_L$, which is ultimately dependent on $\mu$.

The atmospheric heat budgets over land are functions of (1) energy gain at the top of the atmosphere, (2) meridional heat flux between land boxes, and (3) zonal heat flux across the ocean-land boundary:

$$H_{L1} + H_d + \frac{\mu}{(1-\varepsilon)}(T_1 - T_{L1}) = 0 \tag{27}$$

$$H_{L2} - H_d + \frac{\mu}{(1-\varepsilon)}(T_2 - T_{L2}) = 0 \tag{28}$$

The meridional temperature gradient over land is derived from these two equations:

$$T_L = \frac{T_E(2\chi + B) + T\left(\frac{\mu}{(1-\varepsilon)} - 2\varepsilon\chi\right)}{2\chi + B + \frac{\mu}{(1-\varepsilon)} - 2\varepsilon\chi} \tag{29}$$

Now in steady-state:

$$T_L = T + \frac{2|q|(2\chi + B)}{2\chi + B + \frac{\mu}{(1-\varepsilon)} - 2\varepsilon\chi} \tag{30}$$

When there is no flow, $T_L = T_E = T$; when the flow is non-zero, $T_L$'s relationship to $T_E > T$ varies with $\mu$.

*Moisture Over the Ocean and Land*

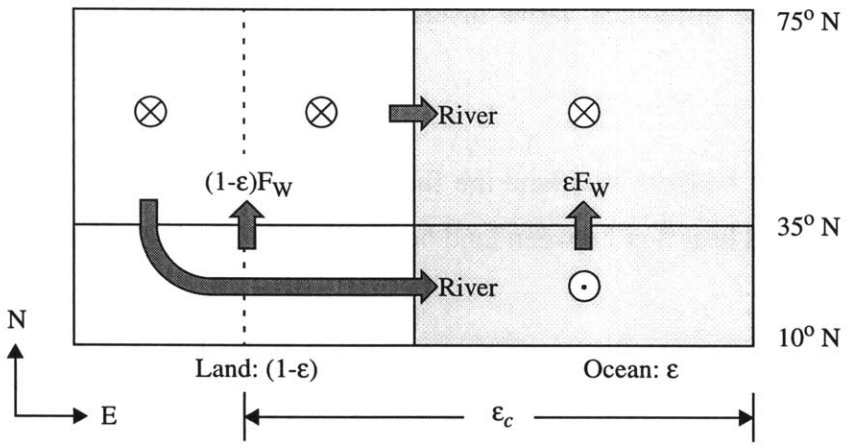


**Figure 3:** Overhead view of surface moisture transports. Poleward meridional transport (in the atmosphere) is split ε over the ocean and (1-ε) over land. Zonal and equatorward meridional transports (in river flow over land) are determined by the catchment area ratio. Smaller $\varepsilon_c$ directs more freshwater to low latitudes where it evaporated; larger $\varepsilon_c$ directs more freshwater to high latitudes where it precipitated.

The atmospheric moisture budget is composed of net evaporation from the low-latitude ocean box and net precipitation into the high-latitude ocean and land boxes. Precipitation falls uniformly around a latitude circle but the portion over land is directed back into the high- and low-latitude ocean boxes through zonal and meridional river flow. The ratio $\varepsilon_W$ of the ocean area to the precipitation catchment area $\varepsilon_c$ is defined so that when $\varepsilon_W = 1$, the catchment area equals the ocean area and freshwater is directed to low latitudes where it evaporated. This counteracts the atmospheric water transport cycle. When $\varepsilon_W = \varepsilon$, the catchment area is the full latitude circle and freshwater is directed to high latitudes where it precipitated. This case retains the full effect of the atmospheric transport. When the catchment area is halfway between ocean area and full circle, half of the precipitation is transported between boxes and half returns to the originating low-latitude basin (shown in figure 3). Evaporation minus precipitation $E$ is then:

$$E = \frac{1}{\varepsilon_W} \frac{F_W}{area} \tag{31}$$

Combining this with the previous definitions of surface salinity flux (eq. 9) and atmospheric moisture transport (eq. 14):

$$H_S = \frac{1}{\varepsilon_W}\frac{S_0}{D}\gamma[T] \tag{32}$$

Note that $\gamma$ equals $\tilde{\gamma}$ divided by the total box area. Now rewrite the meridional mean temperature contrast as:

$$[T] = \frac{1}{\varepsilon_L}\left(\varepsilon T + (1-\varepsilon)\frac{T_E(2\chi + B)}{B + \dfrac{\mu}{\varepsilon(1-\varepsilon)}}\right) \tag{33}$$

and the prognostic equation for meridional salinity difference (combine eqs. 5, 6 and 8 with 32 and 33) is:

$$\dot{S} = 2H_S - 2|q|S = \frac{2}{\varepsilon_W}\frac{S_0}{D}\frac{\gamma}{\varepsilon_L}\left(\varepsilon T + (1-\varepsilon)\frac{T_E(2\chi + B)}{B + \dfrac{\mu}{\varepsilon(1-\varepsilon)}}\right) - 2k|\alpha T - \beta S|S \tag{34}$$

## 2.3 Equilibrium Solutions

To find the steady solutions, set $\dot{T} = 0$ and $\dot{S} = 0$ and solve for $\overline{T}$ (see Appendix A for the derivations). For $q > 0$:

$$\overline{T}_T = \frac{(2k\beta S - \lambda_L) + \sqrt{(2k\beta S - \lambda_L)^2 + 8k\alpha\lambda_L T_E}}{4k\alpha} \tag{35}$$

$$\overline{T}_S = \frac{-k\alpha S_{crit}\left(\dfrac{(1-\varepsilon)}{\varepsilon}\dfrac{T_E(2\chi + B)}{B + \dfrac{\mu}{\varepsilon(1-\varepsilon)}}\right) - k\beta S^2}{k\alpha(S_{crit} - S)} \tag{36}$$

where the critical salinity above which the steady solutions lie is defined as:

$$S_{crit} = \frac{1}{k\alpha D}\frac{\gamma}{\varepsilon_W}\frac{\varepsilon}{\varepsilon_L}S_0 \tag{37}$$

For a steady-state to exist between 0 and $S_{crit}$, the high-latitude box would have to be warmer than the low-latitude box in equilibrium; a decidedly unrealistic outcome. The equations are more readily analyzed in graphical form (figure 4 and table 1).

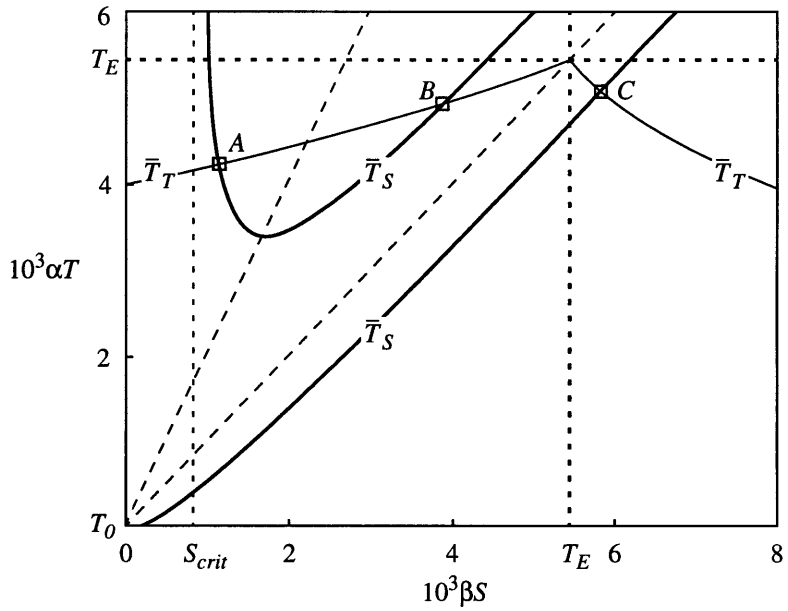


**Figure 4:** T-S phase-space for $\mu = \infty$; all other parameters at default values. Curves $\bar{T}_T$ and $\bar{T}_S$ respectively represent $\dot{T} = 0$ and $\dot{S} = 0$. Along the diagonal $\alpha T = \beta S$ there is no oceanic flow. To the left, flow is poleward near the surface; to the right, flow is equatorward near the surface. The diagonal $\alpha T = 2\beta S$ meets the poleward flow branch of $\bar{T}_T$ at its minimum. Where temperature and salinity curves intersect, *A* (stable) and *B* (unstable) represent temperature-dominated and *C* (stable) represents salinity-dominated steady-states.

The diagonal $\alpha T = \beta S$ represents temperature and salinity balance where there is no flow. To the left of this line, the flow is dominated by temperature: water moves poleward near the surface ($q > 0$) to sink at high latitudes due to its decrease in temperature. To the right, the flow is dominated by salinity: water moves equatorward near the surface ($q < 0$) to sink at low latitudes due to its gain in salinity. $\dot{T} = 0$ and $\dot{S} = 0$ curves meet at the steady solutions: *A* (stable) and *B* (unstable) have poleward flows and *C* (stable) has an equatorward flow. The existence and geometry of these equilibria vary with the choice of parameter values or atmospheric model (linear or non-linear). We now turn to exploring these equilibria and their stability.

| Symbol | Value | Definition |
|---|---|---|
| $A_1$ | -39 $Wm^{-2}$ | High-latitude radiative forcing |
| $A_2$ | 91 $Wm^{-2}$ | Low-latitude radiative forcing |
| B | 1.7 $Wm^{-2}$ $K^{-1}$ | Longwave radiation coefficient |
| $\chi$ | 1.3 $Wm^{-2}$ $K^{-1}$ | Atm meridional heat transport efficiency |
| $\gamma$ | $2.8\times10^{-10}$ $ms^{-1}K^{-1}$ | Atm meridional moisture transport efficiency |
| $\mu$ | $\infty$ $Wm^{-2}$ $K^{-1}$ | Atm zonal heat transport efficiency |
| area | $1.25\times10^{14}$ $m^2$ | Total high-latitude area |
| e | 0.5 | Fractional ocean area |
| $\varepsilon_W$ | 0.5 | Fractional catchment area |
| $\alpha$ | $1.8\times10^{-4}$ $K^{-1}$ | Thermal expansion coefficient |
| $\beta$ | $0.8\times10^{-3}$ $psu^{-1}$ | Haline expansion coefficient |
| k | $2\times10^{-8}$ $s^{-1}$ | Hydraulic constant |
| $\rho_0 c$ | $4\times10^{6}$ $Jm^{-3}K^{-1}$ | Heat capacity of a unit water column |
| D | $5\times10^{3}$ m | Ocean depth |

**Table 1:** Parameters and their default values. The default (infinite) value for zonal heat transport efficiency leads the model to behave as described in Marotzke (1996).

# 3 Equilibrium Analysis

## 3.1 Parameter Influence

Multiple equilibria exist because the ocean's overturning $q$ can be positive, negative or zero. To understand how parameters can lead to different steady-states and their relation to each other, we trace changes in values through their effect on $\bar{T}_T$ and $\bar{T}_S$. Let's initially consider atmospheric zonal heat transport $\mu$ to be infinitely efficient. Later we will relax this restriction and compare the effects of finite $\mu$ against the other parameter changes. The temperature over land $T_L$ therefore converges to the ocean temperature $T$. Global surface temperatures and meridional heat and moisture transports are determined only by the ocean. The effective ocean area ratio $\varepsilon_L$ converges to the ocean area ratio $\varepsilon$ and the Newtonian damping coefficient $\lambda_L$ becomes:

$$\lambda_L = \frac{1}{\varepsilon}\left(\frac{2\chi + B}{c\rho_0 D}\right) \tag{38}$$

The equation for $\bar{T}_T$ (eq. 35) otherwise remains unchanged. Thus the only link between zonal mixing efficiency and the equilibrium temperature gradient is through the restoring coefficient. The ocean area ratio effectively scales the restoring strength between its minimum at $\varepsilon = 1$ and its maximum (infinite strength) at $\varepsilon = 0$. With the equivalence of $\varepsilon_L$ and $\varepsilon$, the critical salinity $S_{crit}$ becomes:

$$S_{crit} = \frac{1}{k\alpha D}\frac{\gamma}{\varepsilon_W}S_0 \tag{39}$$

and the equation for $\bar{T}_S$ (eq. 36) reduces to:

$$\bar{T}_S = -\frac{k\beta S^2}{k\alpha(S_{crit} - S)} \tag{40}$$

Poleward and equatorward flow branches of both equilibrium curves meet at $\alpha T = \beta S$, where there is no flow. At this point on $\bar{T}_T$, the maximum equilibrium temperature contrast is $T_E$; on $\bar{T}_S$, the minimum temperature contrast is $T_0 = 0$.

***Area Ratios***

As the ocean area ratio $\varepsilon \to 0$, $\lambda_L$ becomes stronger and $\bar{T}_T$ shifts upward to $T_E$, the equilibrium that ignores the ocean's role in heat transport. A smaller ocean cools more quickly and flow dynamics have less influence than radiative balance on the steady-state temperature contrast. As $\varepsilon \to 1$, $\lambda_L$ becomes weaker and $\bar{T}_T$ shifts downward while remaining anchored at $\alpha T_E = \beta S$. Now the ocean covers the planet and has a greater influence on the temperature contrast. Continue increasing $\varepsilon$ greater than 1, and $\bar{T}_T$ and $\bar{T}_S$ will no longer meet to form a temperature-dominated solution. The result is a single salinity-dominated steady-state that remains relatively constant even as $\varepsilon$ becomes quite large, due to the anchoring at $T_E$.

As the ocean area to precipitation catchment area ratio $\varepsilon_W \to \varepsilon$, $S_{crit}$ increases and $\bar{T}_S$ shifts outward from the diagonal $\alpha T = \beta S$ (the poleward flow branch moves up along $0.5\alpha T = \beta S$; the equatorward flow branch moves down). The minimum remains $\alpha T_0 = \beta S$. A larger relative catchment area means equatorward river runoff has greater influence on the salinity contrast. The flow to low-latitudes offsets net precipitation in high-latitudes, so less water is transported between ocean boxes. The net impact is a larger meridional salinity gradient. Continue decreasing $\varepsilon_W$ lower than $\varepsilon$ and the temperature-dominated solution vanishes. The result is a single salinity-dominated steady-state. As $\varepsilon_W \to 1$, $S_{crit}$ decreases and $\bar{T}_S$ shifts in toward the diagonal $\alpha T = \beta S$. Now river runoff has less influence on the salinity contrast. With $\varepsilon_W$ increasingly larger than 1, two steady-states in temperature-salinity balance (no flow) result: one at $\alpha T_0 = \beta S$ which is stable and one at $\alpha T_E = \beta S$ which is unstable.

Bear in mind that varying $\varepsilon$ while holding $\varepsilon_W$ constant changes the percentage of freshwater flux carried meridionally by the land. For example, if $\varepsilon$ and $\varepsilon_W$ are initially non-zero and equal, land

plays no role in moisture transport between ocean boxes. Decreasing ε alone introduces a new feedback as precipitation and river flow now carries water equatorward. To isolate the effects of changes only in the ocean area ratio, the catchment area should be set so:

$$\varepsilon_W = \frac{\varepsilon}{\varepsilon + R(1-\varepsilon)} \tag{41}$$

where $R$ is the desired ratio of meridional to zonal river flow.

***Atmospheric Transport Efficiencies***

As the meridional heat transport efficiency $\chi$ decreases, $\lambda_L$ becomes weaker while $T_E$ increases. Smaller $H_d$ thus reduces the atmosphere's ability to balance a temperature contrast so $T$ equilibrates more slowly. As $T_E$ is determined by heat transport and radiative terms, a decrease in the former can be offset by a net increase in the latter. $\chi \to 0$ leads $T_E$ to be determined by radiative balance alone, so:

$$T_R \equiv T_E\big|_{\chi=0} = \frac{A_2 - A_1}{B} \tag{42}$$

As $\chi$ increases, $\lambda_L$ becomes stronger while $T_E$ decreases. The damping shifts $\overline{T}_T$ toward $T_E$, only now the cause is increased transport efficiency rather than decreased ocean area. With the decrease in $T_E$, $\overline{T}_T$ shifts downward. Holding the radiative forcing terms constant, increasingly efficient $\chi$ will lead to a single salinity-dominated steady-state. Equilibrium $T$ and $S$ will be smaller than for the other steady-states, due to the atmosphere's ability to balance the temperature contrast. Recall that both $\overline{T}_T$ and $\overline{T}_S$ are directly related to $T_E$ (eqs. 35 and 36).

As the meridional moisture transport efficiency $\gamma$ decreases, $S_{crit}$ decreases and $\overline{T}_S$ shifts inward toward the diagonal $\alpha T = \beta S$. Smaller $F_W$ thus reduces the atmosphere's ability to balance a salinity contrast so $S$ equilibrates more slowly. The result is familiar because $\gamma$ and $\varepsilon_W$ appear in the definition of $S_{crit}$ as a ratio; a decrease in $\gamma$ is mathematically equivalent to an increase in $\varepsilon_W$. $\gamma \to 0$ leads to the two steady-states in temperature-salinity balance: stable at $T_0$ and unstable at $T_E$. As $\gamma$ increases, $S_{crit}$ increases and $\overline{T}_S$ shifts outward from the diagonal $\alpha T = \beta S$. This

increases the atmosphere's role in moisture transport and is analogous to reducing equatorward river runoff. Increasingly efficient $\gamma$ will lead to the single salinity-dominated steady-state.

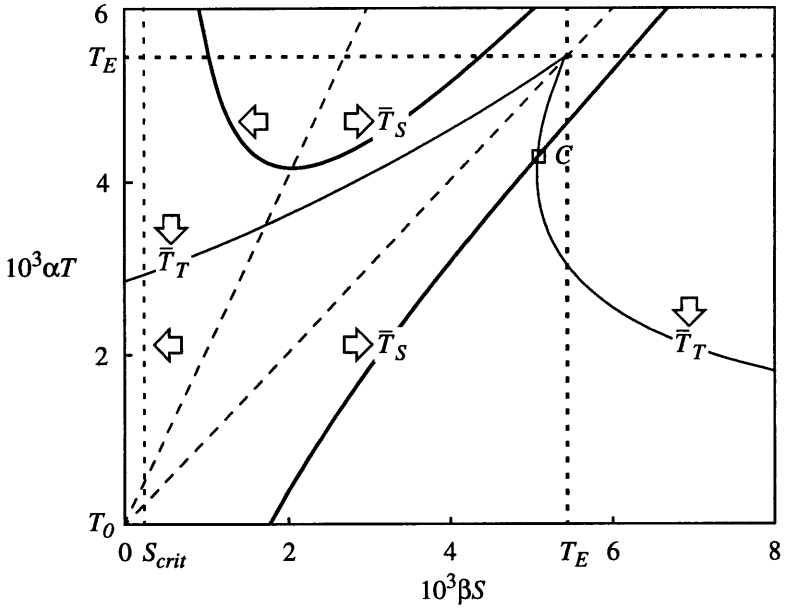


**Figure 5:** T-S phase space with $\mu \equiv 0$ ; all other parameters at default values. The arrows indicate the direction $\bar{T}_T$, $\bar{T}_S$ and $S_{crit}$ curves move as $\mu$ is decreased. Only the salinity-dominated steady-state $C$ remains. At $C$, $\alpha T_E > \beta S$, an outcome not possible for the equatorward flow steady-state with infinite $\mu$.

Now let's allow finite zonal heat transport $\mu$ (figure 5). The first-order effect is that land and ocean temperatures no longer must equal each other. We can think about $\mu$'s effect on meridional temperature gradients over land and the ocean by observing $T_L$ - $T$. The difference should be at a maximum when $\mu = 0$, so:

$$(T_L - T)_{max} = \frac{2\chi + B}{B + 2\chi(1-\varepsilon)}(T_E - T) \tag{43}$$

which is greater than ($T_E$ - $T$). It follows that $T_L > T_E$. Recall that as long as there is a non-zero ocean flow, $T_E > T$. So we now have $T_L > T_E > T$. With finite $\mu$, as long as an ocean exists and has non-zero flow, the temperature gradient over land will be larger than would occur with no ocean (or flow) at all (figure 6).

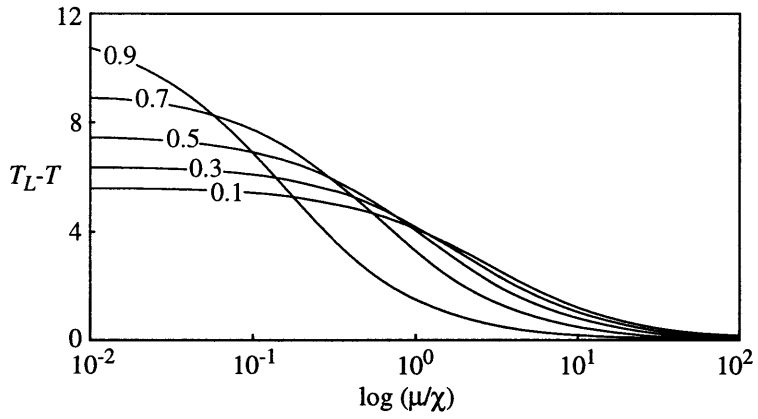


**Figure 6:** ($T_L$ - $T$) versus log (μ/χ) for several values of ε. The default $T$ is 25 °C. For smaller μ and larger ε, the divergence between the temperature gradients over land and ocean increases.

The decrease in μ also leads to an increase in $\varepsilon_L$ and thus a weaker $\lambda_L$. As before, $\overline{T}_T$ shifts downward from $T_E$ while remaining anchored at $\alpha T_E = \beta S$. The equatorward flow branch shifts so that $\alpha T_E$ can be greater than $\beta S$ in equilibrium, a result not possible with infinite zonal mixing. The equilibrium ocean temperature gradient responds to the decrease in μ exactly as to an increase in ε greater than 1. Finite zonal mixing thus provides a physical interpretation of further increasing the ocean area ratio and allowing weaker restoring. The largest effective ocean area occurs when μ = 0, so:

$$\varepsilon_{L,\,max} = \frac{B + 2\chi(1-\varepsilon)}{B} \tag{44}$$

and the divergence between $\varepsilon_L$ and ε increases as the ocean becomes smaller (figure 7):

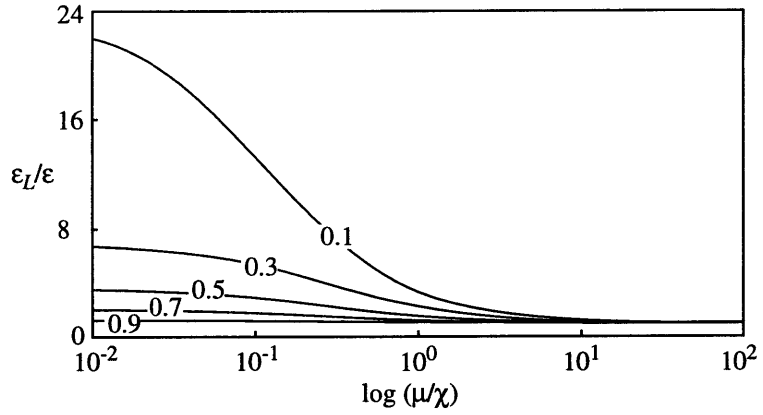


**Figure 7:** ($\varepsilon_L/\varepsilon$) versus log ($\mu/\chi$) for several values of $\varepsilon$. The default $T$ is 25 °C. For smaller $\mu$ and $\varepsilon$, the divergence between actual and effective ocean area ratios increases.

Land temperatures become less responsive to the ocean's temperature gradient as ocean size decreases. Meridional heat and moisture transports then also become more dependent on land temperatures. So assuming perfect zonal mixing leads us to over-estimate the ocean area or meridional heat transport that leads to the single salinity-dominated steady-state.

Turning to salinity, the increase in $\varepsilon_L$ decreases $S_{crit}$. $\overline{T}_S$ flattens horizontally around $T_E$, which is manifest in an upward shift of the poleward flow branch and a rightward shift of the equatorward flow branch. Note that the equilibrium salinity gradient no longer must pass through the origin. The result is that an equatorward flowing steady-state is possible where there is a mean meridional temperature contrast, but no purely oceanic temperature contrast. The mean contrast then equals $(1\text{-}\varepsilon)T_L$. The largest salinity gradient in this situation occurs when $\mu = 0$. For $q > 0$:

$$S|_{\overline{T}=0} = \sqrt{\frac{S_0\gamma}{\beta\varepsilon_W}\frac{(1-\varepsilon)}{\varepsilon_L}\frac{T_E(2\chi+B)}{B}} \tag{45}$$

and the divergence between this $S$ and 0 increases as $\varepsilon$ decreases. Qualitatively this affects the system's behavior only slightly, since the rightward shift in $\overline{T}_S$ occurs in the triangle below $\alpha T_E = \beta S$, a region where no stable equilibria exist. The strongest influence on stability would be the case where $T_E$ were quite small (due to say, large $\chi$). This would effectively place the shifted portion of the curve to the right of $\alpha T_E = \beta S$, the region where the salinity-dominated steady-state

exists. While this equilibrium will then have a larger salinity contrast than with infinite zonal mixing, it remains stable. This makes sense, since a larger salinity gradient encourages the equatorward flow state. As the zonal mixing efficiency decreases, changes in the ocean area ratio or meridional heat transport increasingly affect equilibrium salinities, where before they only influenced temperatures. This tighter coupling leads the system to be more sensitive to parameter variations, an indicator of decreased stability. Assuming perfect zonal mixing thus also leads us to under-estimate the precipitation catchment area or meridional moisture transport that leads to the single salinity-dominated steady-state.

***Atmospheric Models***

The preceding analysis has been based on linear atmospheric transports. Moving to the general (non-linear) atmospheric models result in different analytical solutions for the steady-states. For small atmospheric heat and moisture transport anomalies, we can linearize around the equilibrium mean temperature gradient:

$$H'_d \equiv H_d(\overline{[T]} + [T]') - H_d(\overline{[T]}) = \tilde{\chi}_n(\overline{[T]} - [T]')^n - \tilde{\chi}_n\overline{[T]}^n \tag{46}$$

$$F'_W \equiv F_W(\overline{[T]} + [T]') - F_W(\overline{[T]}) = \tilde{\gamma}_m(\overline{[T]} - [T]')^m - \tilde{\gamma}_m\overline{[T]}^m \tag{47}$$

The mean meridional transports in steady-state are defined to be the same for any $n$ or $m$, so all models will have the same surface fluxes and flow field. In this case:

$$H'_d(T) \cong n\tilde{\chi}_1[T]' = n\tilde{\chi}_1\frac{\varepsilon}{\varepsilon_L}T' \tag{48}$$

$$F'_W(T) \cong m\tilde{\gamma}_1[T]' = m\tilde{\gamma}_1\frac{\varepsilon}{\varepsilon_L}T' \tag{49}$$

Thus atmospheric transports vary $n$ and $m$ times the linear values for a particular perturbation of the meridional mean or ocean (from eq. 33) temperature gradient. Newtonian damping is then:

$$\lambda_L = \frac{1}{\varepsilon_L}\left(\frac{2n\chi + B}{c\rho_0 D}\right) \tag{50}$$

so a smaller $n$ results in weaker restoring. As $n$ decreases, $\lambda_L$ decreases and eventually heat transport becomes fixed for any $T$. This results in $\overline{T}_T$ moving downward, similar to an increase in $\varepsilon$ or decrease in $\chi$. Each results in less efficient heat transport. As $m$ decreases, $S_{crit}$ increases and eventually moisture transport becomes fixed. This results in $\overline{T}_S$ moving upward, similar to an increase in $\varepsilon_w$ or decrease in $\gamma$. Each of these changes results in less efficient moisture transport.

## 3.2 Feedback Structure

For any equilibrium flow state, the relative strength of the feedbacks largely determines whether the system remains stable or makes a transition to another state. To determine the model's feedbacks, we linearize ocean flow and atmospheric transport equations around the equilibrium steady-states $T = (\overline{T} + T')$, $S = (\overline{S} + S')$ and $q = (\overline{q} + q')$. Keeping only the first-order terms, for $q > 0$:

$$\dot{T}' \equiv \dot{T}(\overline{T} + T') - \dot{T}(\overline{T}) \cong H'_T(T') - 2q'\overline{T} - 2\overline{q}T' \tag{51}$$

$$\dot{S}' \equiv \dot{S}(\overline{T} + T') - \dot{S}(\overline{T}) \cong H'_S(T') - 2q'\overline{S} - 2\overline{q}S' \tag{52}$$

where:

$$q' = k(\alpha T' - \beta S') \tag{53a}$$

$$\overline{q} = k(\alpha \overline{T} - \beta \overline{S}) \tag{53b}$$

and:

$$H'_T(T') \cong -\frac{1}{\varepsilon_L}\left(\frac{2n\chi + B}{c\rho_0 D}\right)T' \tag{54}$$

$$H'_S(T') \cong \frac{\varepsilon}{\varepsilon_L}\frac{2m\gamma S_0}{\varepsilon_W D}T' \tag{55}$$

Then trace a perturbation in $T'$ through the equations. Balancing (negative) feedback weakens the behavior caused by a perturbation; reinforcing (positive) feedback strengthens the behavior. The first four feedbacks this identifies are strictly oceanic. Mean flow (right-hand term in eqs. 51 and 52) reduces variations in $T$ or $S$ and is therefore balancing.


**Figure 8a:** Feedback loops for mean flow, the ocean's tendency to reduce variations in temperature and salinity. They represent the right-hand terms in eqs. 51 and 52. Both are balancing and therefore stabilize the equilibria.

Ocean heat transport (mid term in eq. 51) reduces variations in $T$ given surface heat transport. Ocean salinity transport (mid term in eq. 52) increases variations in $S$ given surface moisture transport.


**Figure 8b:** Feedback loops for ocean heat and salinity transport. They represent the mid terms in eqs. 51 and 52. Heat transport is balancing and stabilizes the equilibria; salinity transport is reinforcing and destabilizes.

Ignoring all atmospheric effects, it is the ocean salinity transport that leads to more than one steady-state. The following two feedbacks couple atmospheric transports with the ocean flow. Atmospheric heat transport reduces variations in $T$ but also reduces the strength of the ocean heat transport. The loop balances considered strictly in the atmosphere, but reinforces when combined with ocean flow.

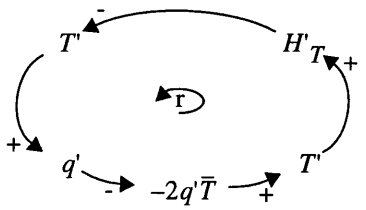


**Figure 8c:** Feedback loop for coupled ocean-atmosphere heat transport. Considered strictly in the atmosphere, the feedback is balancing but when coupled with ocean heat transport feedback (first loop in figure 8b) is reinforcing. The combined feedback destabilizes the model's equilibria in that it counteracts the stabilizing ocean heat transport.

The dominance of ocean or atmospheric heat transport depends on $\lambda_L$. If damping is strong (large $H'_T$), atmospheric heat transport counteracts the ocean's temperature balancing effects; if damping is weak (fixed $H'_T$), atmospheric heat transport is minimal and its destabilizing effect on the ocean's temperature moderation is weak. Atmospheric moisture transport increases variations in $T$ or $S$.

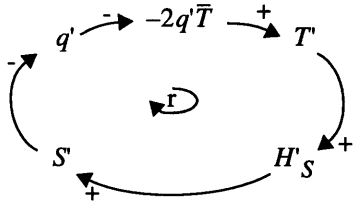


**Figure 8d:** Feedback loop for coupled ocean-atmosphere moisture transport. The feedback is always reinforcing and destabilizes the model's equilibria.

In this case, the efficiency of atmospheric moisture transport does not affect the direct relationship between $T'$ and $S'$ and the feedback is always reinforcing. Taken together, the last four loops give a good representation of model dynamics.

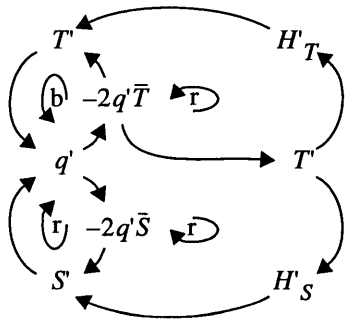


**Figure 8e:** Feedback structure showing ocean and coupled heat and salinity transports.

## 3.3 Equilibrium Stability

The parameter variations in the previous discussion can be categorized as equivalent to increasing meridional atmospheric heat or moisture transports. For heat flux, larger $\varepsilon$ or smaller $\chi$ decreases the temperature equilibration time and emphasizes the vertical structure in $T$-$S$ phase space. For moisture flux, smaller $\varepsilon_L$ or larger $\gamma$ decreases the salinity equilibration time and emphasizes the horizontal structure. As the model is tuned so non-linear atmospheres have the same temperature-

dominated steady-state, varying $n$ and $m$ gives a good representation of alternative transport strength scenarios. Each can readily be evaluated against various zonal mixing efficiencies to find $\mu$'s effect on feedback strengths. However, it is not clear whether the stability characteristics are the same between different atmospheres. We proceed by considering five models corresponding to different powers of $n$ and $m$ (table 2).

| Model | Values | Description |
|---|---|---|
| a | $\chi_0, \gamma_0$ | Radiative balance alone |
| b | $\chi_1, \gamma_1$ | Fully linear atmosphere |
| c | $\chi_1, \gamma_3$ | Linear heat, cubic moisture |
| d | $\chi_3, \gamma_1$ | Cubic heat, linear moisture |
| e | $\chi_3, \gamma_3$ | Fully cubic atmosphere |

**Table 2:** Atmospheric models.

Section 2 on parameter variation shows that the model is inclined to lose the temperature-dominated steady-state (*A* in figure 4) due to changing parameter values or atmospheric transport laws. It is therefore the state we test for stability. Beginning with a 10,000 year spin-up to equilibrium (using $\chi_1$, $\gamma_1$), $\Delta S$ is removed from the high-latitude box and placed into the low-latitude box. The measures of stability to consider are:

- The minimum perturbation $\Delta S_{crit}$ that leads to the salinity-dominated steady-state. Smaller $\Delta S_{crit}$ indicates a less stable model.

- The transition time to the new state for perturbations greater than $\Delta S_{crit}$. A shorter time indicates a less stable model.

- The decay time to the original state for perturbations less than $\Delta S_{crit}$. A longer time indicates a less stable model.

For three sets of trials, zonal heat transport efficiency is varied relative to meridional transport efficiency: (1) $\mu = 10\chi$, (2) $\mu = \chi$ and (3) $\mu = 0.1\chi$. Within each set, there are two separate trials that differ only in the value of $\gamma$ in the spin-up. Atmospheric models are listed in order of decreasing stability represented by $\Delta S_{crit}$ (table 3).

| Model | (1) $\mu = 10\chi$ | | (2) $\mu = \chi$ | | (3) $\mu = 0.1\chi$ | |
|---|---|---|---|---|---|---|
| (n, m) | $\gamma = 2.8$ | $\gamma = 2.2$ | $\gamma = 2.8$ | $\gamma = 2.2$ | $\gamma = 2.8$ | $\gamma = 2.2$ |
| a (0, 0) | 2.20 | 3.34 | 1.39 | 2.27 | 0 | 0.99 |
| b (1, 1) | 1.47 | 1.96 | 0.87 | 1.61 | 0 | 0.66 |
| d (3, 1) | 1.27 | 1.73 | 0.77 | 1.47 | 0 | 0.61 |
| e (3, 3) | 1.10 | 1.60 [5] | 0.61 | 1.3562 [5] | 0 | 0.52 |
| c (1, 3) | 1.09 | 1.65 [4] | 0.55 | 1.3567 [4] | 0 | 0.46 |

**Table 3:** $\Delta S_{crit}$ required for a transition from the temperature-dominated steady-state to salinity-dominated. The table can be read left-to-right for decreasing $\mu$ or $\gamma$ (in alternate columns) or top-to-bottom for decreasing $\Delta S_{crit}$. Bracketed figures indicate the changed order in stability based on $\Delta S_{crit}$. Where values are 0, only the salinity-dominated state remains.

For any model with prescribed zonal heat transport, a larger meridional moisture transport results in smaller $\Delta S_{crit}$, an indicator of less stability. Larger transport also implies increased sensitivity to the value of $m$ in the power law. Increasing $\gamma$ makes the destabilizing atmospheric moisture transport feedback stronger, which agrees with the earlier conclusion that large enough $\gamma$ leads to only the salinity-dominated equilibrium. Just this situation results in trial (3) where $\mu = 0.1\chi$ and $\gamma = 2.8$. The temperature-dominated state is then very unstable indeed.

Alternatively, for any model with prescribed meridional moisture transport, smaller zonal heat transport decreases stability. Recall that decreasing $\mu$ weakens Newtonian damping $\lambda_L$ and thus reduces heat flux $H_T$. The destabilizing (when coupled with ocean circulation) atmospheric heat transport feedback is then weaker. Considered alone, this should increase model stability. But decreasing $\mu$ also decreases $S_{crit}$ and increases $H_S$. The (always) destabilizing atmospheric moisture transport feedback is then stronger. The competing effects can be thought of as follows. As $H_T$ decreases, the atmospheric heat transport feedback only stabilizes the model to the extent that it no longer counteracts the balancing ocean heat transport feedback. It thus affects loop dominance within a certain range specified by the ocean's feedback strength. But as $H_S$ increases, the atmospheric moisture transport continues to destabilize. Taken together, the salinity transport feedback becomes more important as $\mu$ becomes smaller. The full equations for linearized

temperature (combine eqs. 51, 53 and 54) and salinity (combine eqs. 52, 53 and 55) gradient tendencies illustrate these influences:

$$\dot{T}' = -(\lambda_L + 2k\alpha\bar{T} + 2\bar{q})T' + 2k\beta\bar{T}S' \tag{56}$$

$$\dot{S}' = 2k\alpha(mS_{crit} - \bar{S})T' + 2(k\beta\bar{S} - \bar{q})S' \tag{57}$$

By setting $\dot{T}' = 0$ in equilibrium and solving for $T'$, we get:

$$\dot{S}' = \left( \frac{4k^2\alpha\bar{T}\beta(mS_{crit} - \bar{S})}{\lambda_L + 2k\alpha\bar{T} + 2\bar{q}} + 2(k\beta\bar{S} - \bar{q}) \right) S' \tag{58}$$

So a change in parameters that decreases heat transport (say, smaller $\chi$) or increases moisture transport (larger $\gamma$) makes the first (negative) term of $\dot{S}'$ smaller and therefore destabilizes. Decreasing $\mu$ does both by increasing $\varepsilon_L$ and decreasing $S_{crit}$ (section 3.1).

For all trials, the model with fixed atmospheric heat and moisture transports (a) is the most stable. Fixing the heat flux means that the reinforcing atmospheric heat transport feedback is no longer active. Therefore, the balancing ocean heat transport feedback dominates the combined loop. Fixing the moisture flux means that the reinforcing atmospheric moisture transport feedback is also no longer active. Only the oceanic feedbacks are left, with salinity transport the remaining destabilizing factor. If longwave heat loss $B$ is also fixed, all surface fluxes would be prescribed and the atmosphere and ocean would be uncoupled.

Models with linear moisture transport (b and d) are increasingly less stable. Relative to a fully linear atmosphere, the cubic heat transport model has a stronger atmospheric heat transport feedback. This loop destabilizes when coupled with the ocean's heat transport, but only to the point where it counteracts the ocean's temperature balancing ability. Further increases in atmospheric heat transport can not further destabilize, and then the fight for dominance is between mean flow, ocean and atmospheric moisture transports.

Models with cubic moisture transport (c and e) are the least stable of all. Unlike the atmospheric heat transport feedback, the moisture transport feedback always destabilizes. The order of stability between the two models is not consistent in all cases though. For the models with linear moisture transport laws (b and d), increasing atmospheric heat transport destabilizes; but for models with higher-order moisture transport (c and e), stability varies depending on the strength of heat and moisture transports. The linearized salinity gradient tendency (eq. 58) suggests why. As long as $mS_{crit}$ is less than $\bar{S}$, the first term of $\dot{S}'$ remains negative and stabilizes. This is the case for $m \leq 1$. For $m \geq 2$, this is no longer the case. Models with different values for $\gamma$ or $\mu$ have different ratios between $mS_{crit}$ and $\bar{S}$ and therefore may not have the same order of stability. Trial (2) where $\mu = \chi$ and $\gamma = 2.2$ is very close to the bifurcation and so the model is very sensitive.

The time series for flow strength agrees with these expectations (figures 9 and 10).

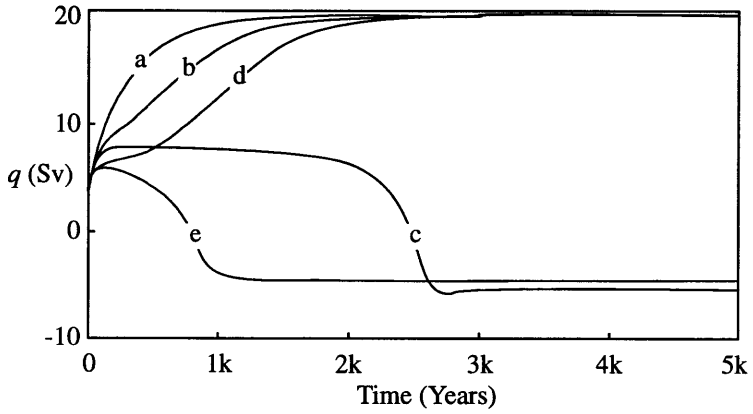


**Figure 8:** Flow strength for trial (1) $\mu = 10\chi$ after a perturbation of 1.65 psu (the $\Delta S_{crit}$ for model c). $\gamma = 2.2\times10^{-10}$ $ms^{-1}K^{-1}$, with all other parameters at default values. Fixed and linear moisture transport models are the most stable. Cubic moisture transport models show (e) takes less time than (c) to make the transition between states, suggesting it is less stable.

For sub-critical perturbations in salinity, the three models with fixed or linear moisture transport return to the temperature-dominated equilibrium in order consistent with the size of $\Delta S_{crit}$. These same models with smaller $\mu$ are given less of an anomaly, but even so, they return to equilibrium much slower while preserving the order of stability.

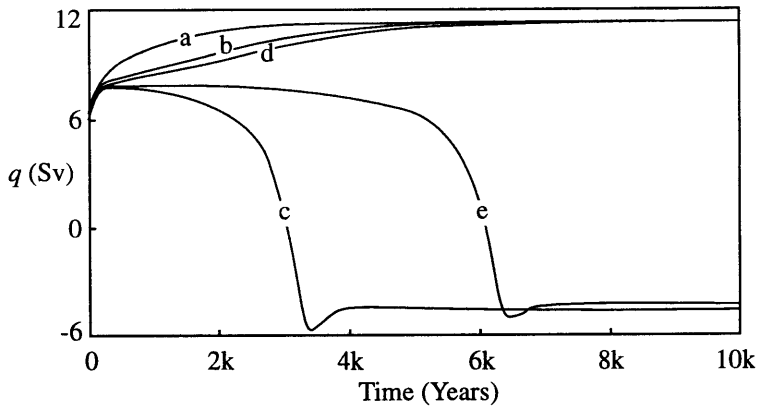


**Figure 9:** Flow strength for trial (3) $\mu = 0.1\chi$ after a perturbation of 0.52 psu (the $\Delta S_{crit}$ for model e). $\gamma = 2.2\times10^{-10}$ $ms^{-1}K^{-1}$, with all other parameters at default values. Again, fixed and linear moisture transport models are the most stable. Cubic moisture transport models show (c) takes less time than (e) to make the transition between states, suggesting it is less stable in this case.

For super-critical perturbations in salinity, the two models with cubic moisture transport make the transition to the salinity-dominated solution in different order depending on the value of $\mu$. In the case with larger m, the model with fully cubic atmosphere (e) is the most unstable, making the transition in less time than the model with linear heat transport (c). But decreasing $\mu$ leads the two models to change their order of stability. This also is consistent with the results using $\Delta S_{crit}$.

Comparing flow strength between figures 8 and 9 also shows how smaller $\mu$ leads to a weaker flow for both equilibria, though more pronounced for the temperature-dominated state. Figure 5, showing the *T-S* phase space with finite $\mu$ explains why. Where $q < 0$, both equilibrium temperature and salinity gradients decrease in response to smaller $\mu$. The heat and moisture transport feedbacks are then both weaker. Where $q > 0$, the equilibrium temperature gradient decreases but the salinity gradient increases in response to smaller $\mu$. In this case, the heat transport feedback (which drives the flow) is weaker and the moisture transport feedback (which counteracts the flow) is stronger.

# 4 Conclusions and Future Work

A simple box model has been developed to explore the influence of limited interaction between the atmosphere over land and the ocean. The ocean consists of two boxes, with heat and salinity transported meridionally through density gradient-induced overturning. The atmosphere consists of four boxes—two over land and two over the ocean—with negligible heat and moisture capacities. Most behavior can be captured through two (temperature and salinity) prognostic equations, which both depend sensitively on the ocean area and atmospheric heat and moisture transport efficiencies.

## 4.1 Bringing the Pieces Together

We started with an atmosphere thoroughly mixed zonally. Temperatures over the ocean then equalled the sea-surface temperatures below, and temperatures over the land equalled those over the ocean at the same latitude. The ocean (as long as it exists) then prescribes all atmospheric temperatures. We then set out to determine how removing this restriction—by varying zonal heat transport efficiency—would change model behavior, especially with respect to the equilibria and feedbacks.

Ocean circulation moderates global temperatures and leads to an equilibrium meridional temperature gradient smaller than would exist without an ocean (that flows). Finite atmospheric zonal heat transport leads to an equilibrium temperature gradient over land that is larger than the gradient over the ocean, and can even be larger than what would exist without an ocean. The larger gradient over land then exerts more control over the global mean meridional temperature

gradient. Ocean basin size then becomes important, as a relatively large ocean still controls the mean gradient but a smaller ocean has weaker damping and land temperatures control the mean.

The mean temperature gradient drives atmospheric meridional heat and moisture fluxes. The larger temperature gradient over land thus leads to larger fluxes, which strengthen the destabilizing atmospheric heat and moisture transport feedbacks. The result is that the model is more sensitive to parameters like the ocean area or atmospheric heat and moisture transports. So assuming infinite zonal transport efficiency causes us to over-estimate the perturbations necessary for a transition between equilibria. As a result, ocean circulation in temperature- and salinity-dominated steady-states is then weaker, though the temperature-dominated equilibrium is affected more strongly. The salinity-dominated state is then a more likely outcome, and an equatorward flowing solution with no oceanic meridional temperature contrast is possible.

While finite zonal transport efficiency increases feedback strength and model sensitivity, assuming infinite transport (and so a zonally uniform atmosphere) is not unreasonable. Allowing the atmospheric temperature gradients over the ocean and land to diverge does not substantially change the equilibrium or feedback structure. Since land temperatures are determined as functions of the meridional temperature gradient (in this formulation), more than the original number of steady-states or feedback loops could not exist. A useful experiment to eliminate the constraint on the number of steady-states would be to independently derive temperatures over land. A GCM approach would allow this as well as indicate whether the increase in temperatures over land due to finite zonal mixing is a robust result.

Further model exploration should focus on the change in model sensitivity with cubic atmospheric moisture transport law. An experiment might use two distinct zonal heat transport efficiencies and vary the moisture transport so that an initial equilibrium were equidistant (measured by the critical salinity) from the bifurcation point around which sensitivity to a critical perturbation varies. This would give a more accurate indication of the magnitude of perturbation required to induce a transition between states, as the starting point would be the same.

## 4.2 Continuing Development

Due to its conceptual simplicity, the box model lends itself well to projects that add functionality and analyze the changes in behavior (like allowing separate temperatures over land). Promising areas for further development might similarly address the model's simplifying assumptions. First is the ocean's uniform density regardless of depth. The simplest approach that balances the salinity is to have the mixing flux proportional to the vertical gradient. This produces prognostic equations for temperature and salinity in shallow and deep layers, thus adding an additional "thermocline" box to each ocean basin.

Second is the lack of albedo. There are two ways of representing temperature-dependent changes in reflectivity: cloud and ice cover. For clouds, the simplest approach is to make the radiative forcing terms at the top of the atmosphere temperature-dependent. The parameterization assumes a direct relationship between temperature and cloud formation, which is feasible but not ideal. Alternatively, the radiative terms could be moisture-dependent. This is more appropriate under general climatic conditions, and can be implemented using the Clausius Clapeyron relation (already included in the numerical model), which relates atmospheric moisture content and transport to the global mean temperature.

For ice, a significant level of cover requires that the ice build up over land (for support) rather than the ocean. As the high-latitude box becomes colder, rain would become snow and a "glacier" would accrete. The increased reflectivity would decrease temperature, thus adding new reinforcing feedback to the system. To maintain the atmosphere's temperature dependence on the sea-surface temperature, longwave radiation could be directly related to ice area coverage. As the area coverage ratio and adjustment timescales are on the order of the ocean's, an additional prognostic equation for ice volume at high-latitude would be required. The area would therefore have to relate directly to volume through some relation. Ice effects become interesting since the salinity flux equations then depend on ocean and atmospheric transports, the volume of the "glacier," and its zonal and meridional meltwater runoff. Ice buildup decreases the ocean's freshwater content, so salinity within the ocean is no longer conserved. As with the current model, precipitation over the ice (which is on land) can be controlled through the catchment area ratio $\varepsilon_W$. However, meltwater flowback would depend on the temperature.

# 5 References

Boyle, E., "Quaternary Deepwater Paleoceanography," *Science* 249 (1990): 863-870.

Broecker, W., Peng, T-P, Jouzel, J. and Russell, G., "The Magnitude of Global Fresh-water Transports of Importance to Ocean Circulation," *Climate Dynamics* 4 (1990):73-79.

Bryan, F., "High-Latitude Salinity Effects and Interhemispheric Thermohaline Circulations," *Nature* 323 (September 25, 1986): 301-304.

*GCM shows that equatorially asymmetric circulation can result from symmetric basin geometry and surface forcing. Multiple equilibria solutions result from perturbation.*

Gordon, A., "Interocean Exchange of Thermocline Water," *Journal of Geophysics Research* 91 (1986): 5037-5046.

*Describes global meridional ocean circulation.*

Manabe, S. and Stouffer, R., , "Two stable equilibria of a coupled ocean-atmosphere model," *Journal of Climate* 1 (1988): 841-866.

*Coupled GCM with two equilibrium solutions.*

Marotzke, J., "Analysis of Thermohaline Feedbacks," *Decadal Climate Variability, Dynamics and Predictability*, Anderson D. and Willebrand, J. eds., NATO ASI Series, vol. I 44 (1996):333-378.

*Four box ocean-atmosphere model including simple formulation for separate temperatures over land. Similar to Marotzke and Stone (1995) but with more complex atmosphere. Model and approach form the basis for this research.*

Marotzke, J. and Stone, P., "Atmospheric Transports, the Thermohaline Circulation, and Flux Adjustments in a Simple Coupled Model," *Journal of Physical Oceanography* 25 no. 6 (June, 1995): 1350-1364.

*Four box ocean-atmosphere model analyzed for equilibria, stability and flux adjustments. Ocean model based on Stommel (1961).*

Marotzke, J. and Willebrand, J., "Multiple Equilibria of the Global Thermohaline Circulation," *Journal of Physical Oceanography* 21 (1991): 1372-1385.

*GCM with two basins investigates equilibria of global thermohaline circulation. Four stable steady states found under same set of boundary conditions.*

Stommel, H., "Thermohaline Convection with Two Stable Regimes of Flow," *Tellus* 13 (1961): 224-230.

*Four box oceanic thermohaline circulation feedback model.*

Warren, B., "Deep Circulation of the World Ocean," *Evolution of Physical Oceanography, Scientific Surveys in Honor of Henry Stommel*, Warren, B. and Wunsch, C., (eds.) Cambridge, MA: MIT Press (1981): 6-41.

*Describes history and recent conceptual models of layered oceanic fluid transports.*

Winton, M., "The Effect of Cold Climate upon North Atlantic Deep Water Formation in a Simple Ocean-Atmosphere Model," *Journal of Climate* (January, 1997): 37.

*Differs from Marotzke in its treatment of land-sea boundary thermal efficiency.*

# 6 Appendices

# A: Derivation of Steady-State Solutions

Following are brief guides through the derivation of equilibrium temperature gradient curves $\bar{T}_T$ and $\bar{T}_S$.

## A.1 Temperature

Set $\dot{T} = 0$ and solve for $T$ ($q > 0$):

$$\lambda_L(T_E - T) - 2k(\alpha T - \beta S)T = 0 \tag{25}$$

Combine like terms:

$$2k\alpha T^2 - (2k\beta S - \lambda_L)T - \lambda_L T_E = 0$$

Apply the quadratic formula:

$$\bar{T}_T = \frac{(2k\beta S - \lambda_L) + \sqrt{(2k\beta S - \lambda_L)^2 + 8k\alpha\lambda_L T_E}}{4k\alpha} \tag{35}$$

And for ($q < 0$):

$$\bar{T}_T = \frac{(2k\beta S + \lambda_L) \pm \sqrt{(2k\beta S + \lambda_L)^2 - 8k\alpha\lambda_L T_E}}{4k\alpha}$$

## A.2 Salinity

Set $\dot{S} = 0$ and solve for $T$ ($q > 0$):

$$\frac{2}{\varepsilon_W}\frac{S_0}{D}\frac{\gamma}{\varepsilon_L}\left(\varepsilon T + (1-\varepsilon)\frac{T_E(2\chi + B)}{B + \frac{\mu}{\varepsilon(1-\varepsilon)}}\right) - 2k(\alpha T - \beta S)S = 0 \tag{34}$$

Combine like terms:

$$\left(\frac{2}{\varepsilon_W}\frac{S_0}{D}\frac{\gamma}{\varepsilon_L}\varepsilon - 2k\alpha S\right)T = -\frac{2}{\varepsilon_W}\frac{S_0}{D}\frac{\gamma}{\varepsilon_L}\left((1-\varepsilon)\frac{T_E(2\chi + B)}{B + \frac{\mu}{\varepsilon(1-\varepsilon)}}\right) - 2k\beta S^2$$

Substitute the definition for $S_{crit}$ and isolate $T$:

$$\overline{T}_S = \frac{-k\alpha S_{crit}\left(\frac{(1-\varepsilon)}{\varepsilon}\frac{T_E(2\chi + B)}{B + \frac{\mu}{\varepsilon(1-\varepsilon)}}\right) - k\beta S^2}{k\alpha(S_{crit} - S)} \tag{36}$$

And for ($q < 0$):

$$\overline{T}_S = \frac{-k\alpha S_{crit}\left(\frac{(1-\varepsilon)}{\varepsilon}\frac{T_E(2\chi + B)}{B + \frac{\mu}{\varepsilon(1-\varepsilon)}}\right) + k\beta S^2}{k\alpha(S_{crit} + S)}$$

# B: Program Code and Model Diagrams

## B.1 Analytical Model Code

The analytical model is implemented in MATLAB. It is relatively straightforward; about half the code is devoted to defining parameters and plotting routines. Parameters are set to default values.

```
%  tsphase.m by David Sirkin, May 01 1998
%  creates a T-S phase plot

%  initialized parameters

   A1=-39;          % surf s/w rad forcing
   A2=91;           % surf s/w rad forcing
   B=1.7;           % surf l/w rad coeff

   chi=1.3;         % atmos merid heat mix eff
   mu=1.3e10;       % atmos zonal heat mix eff
   gam=2.8e-10;     % atmos merid moisture mix eff

   eps=0.5;         % ocean area to total
   epw=0.5;         % ocean area to catchment

   alp=1.8e-4;      % thermal expansion coeff
   bet=0.8e-3;      % haline expansion coeff

   k=2e-8;          % hydraulic constant
   rc=4e6;          % unit vol heat capacity
   D=5e3;           % ocean depth

%  derived parameters

   epl=(B+2*chi*(1-eps)+mu/(1-eps))./(B+mu/(eps*(1-eps)));
   lml=(2*chi+B)./(epl*rc*D);

   So=34;
   S=0:0.1:10;
   Sc=(1/epw)*(So/D)*gam*(eps/epl)*(1/(k*alp));

   TE=(A2-A1)/(2*chi+B);

%  T=0 (TT) and S=0 (TS) curves
%  p=poleward flow branch & e=equatorward flow branch
%  for T=0 e branch only, a has pos root & b has neg root

   TTp =((2*k*bet*S-lml)+sqrt(((2*k*bet*S-lml).^2)...
         +8*k*alp*lml*TE))/(4*k*alp);
   TTea=((2*k*bet*S+lml)+sqrt(((2*k*bet*S+lml).^2)...
         -8*k*alp*lml*TE))/(4*k*alp);
   TTeb=((2*k*bet*S+lml)-sqrt(((2*k*bet*S+lml).^2)...
         -8*k*alp*lml*TE))/(4*k*alp);
```

```
    TSp=(-k*alp*Sc*((1-eps)/eps)*TE*(2*chi+B)/(B+mu/(eps*(1-eps)))...
        -(k*bet*(S.^2)))./(k*alp*(Sc-S));
    TSe=(-k*alp*Sc*((1-eps)/eps)*TE*(2*chi+B)/(B+mu/(eps*(1-eps)))...
        +(k*bet*(S.^2)))./(k*alp*(Sc+S));

%   find critical points to define plotting range for TT

    te=sum(alp*TE>bet*S);      % alp*TE for p and e branches
    im=sum(imag(TTea)>0);      % imaginary limit for e branch
    ln=length(TTea);           % final value for e branch

%   don't plot segments of TT where e>alp*TE

    if alp*TTea(im+1)>alp*TE, im=te; end

%   salinity (x-axis) and temperature (y-axis) vectors for the figure

    sv=1e3*bet*S;
    tv=1e3*alp;

%   plot T-S phase

    figure
    hold on

    plot(sv(1:te),tv*TTp(1:te),'r-');
    plot(sv(im:te),tv*real(TTea(im:te)),'r-');
    plot(sv(im:ln),tv*real(TTeb(im:ln)),'r-');
    plot(sv,tv*TSp,'b-',sv,tv*TSe,'b-');

    axis([0 8 0 6]);
    title('T-S Phase Diagram');
    xlabel('10^3betaS'); ylabel('10^3alphaT');

%   add landmarks to figure

    plot(sv,sv,'k:',sv,2*sv,'k:');
    line([0 8],[tv*TE tv*TE],'Color','k','LineStyle','--');
    line([tv*TE tv*TE],[0 6],'Color','k','LineStyle','--');
    text(tv*TE-0.1,-0.175,'TE'); text(-0.275,tv*TE,'TE');
    text(1e3*bet*Sc-0.1,-0.175,'Sc');

%   add legend of derived values

    patch([6 7.75 7.75 6],[0.25 0.25 1 1],'w');
    text(6.25,0.65,['eps_L = ',num2str(epl,3)]);
    text(6.25,0.40,['lam_L = ',num2str(lml,3)]);

    hold off

%   housekeeping

    return
```

## B.2 Numerical Model Diagrams and Code

The numerical model is implemented in MATLAB's Simulink environment. Changes in the feedback structure or subroutine definition are therefore relatively straightforward. Following are the main structural and subroutine diagrams; they are accompanied by variable definitions where required.

Outer loop:

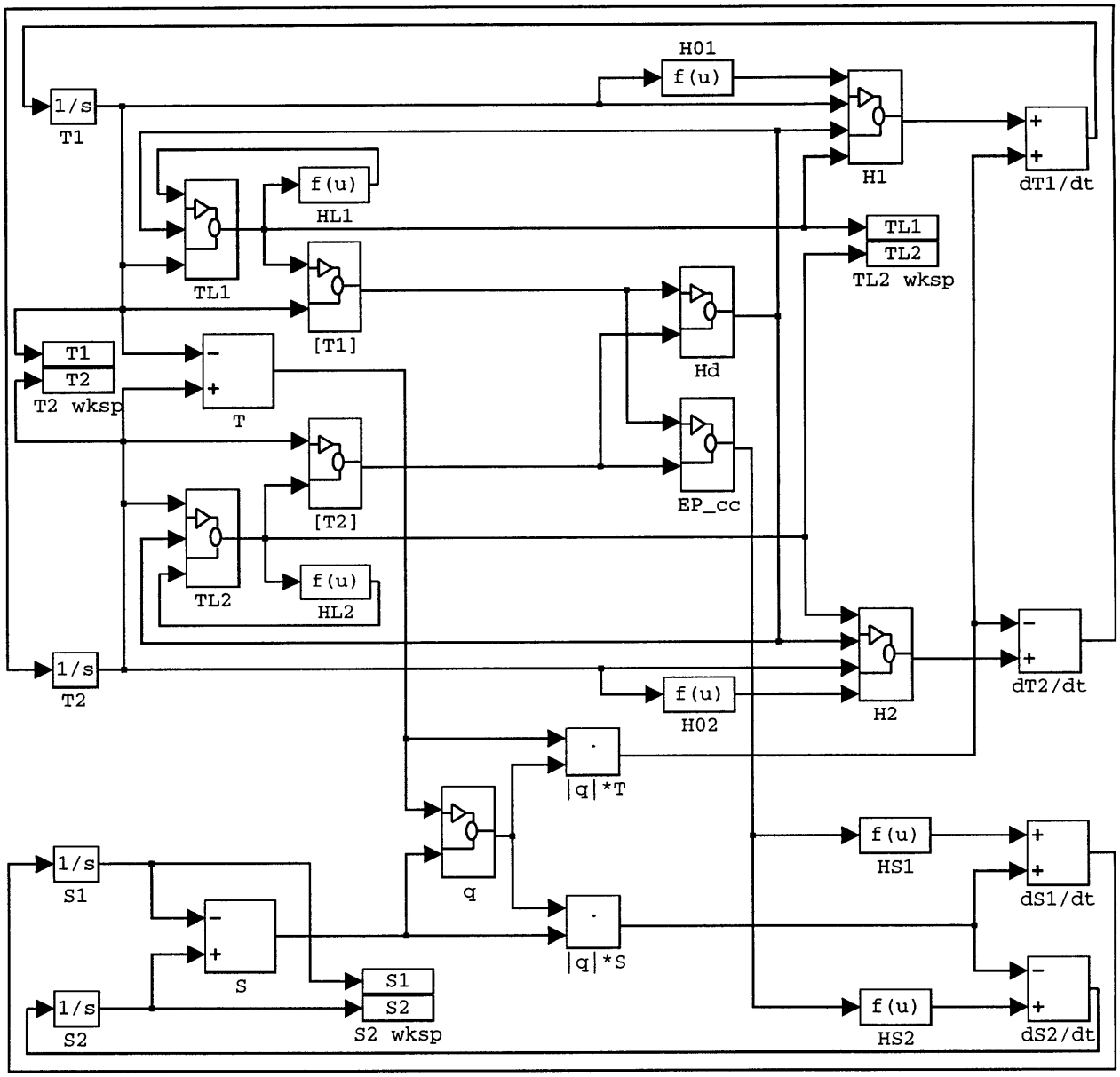

Ocean flow strength:

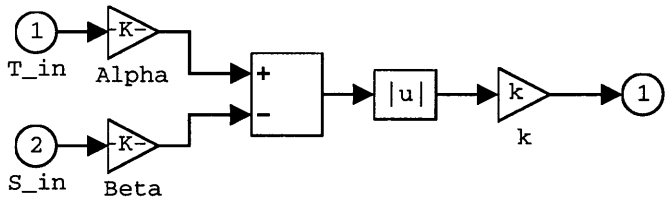


Mean meridional temperatures:

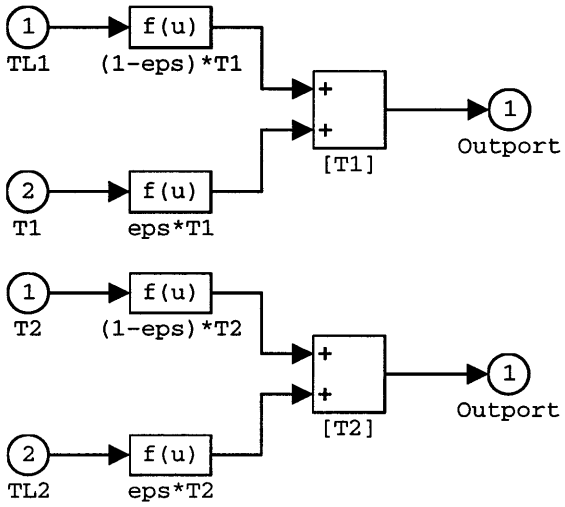


Mean meridional atmospheric heat transport:

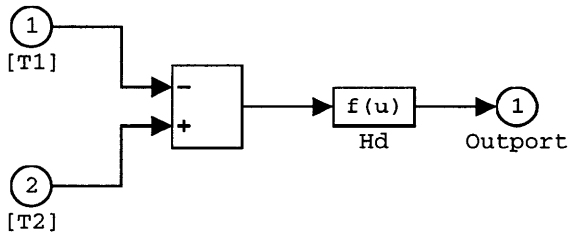


where `Hd=chi_n*u[1]^n`

Mean meridional atmospheric moisture transport including Clausius Clapeyron effect:

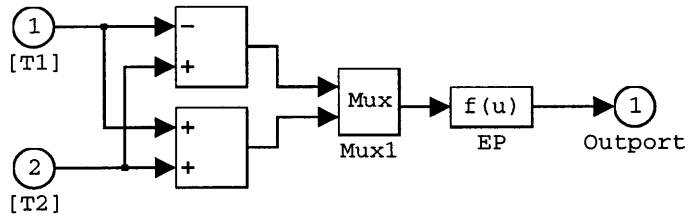


where `EP=gamma_m*(u[1]^m)/ew*(1-p_cc+p_cc*(273+TMEstd)/(273+u[2]/2)*...`
`exp(-5420*(1/(273+u[2]/2)-1/(273+(TMEstd)))))`

Temperatures over land:

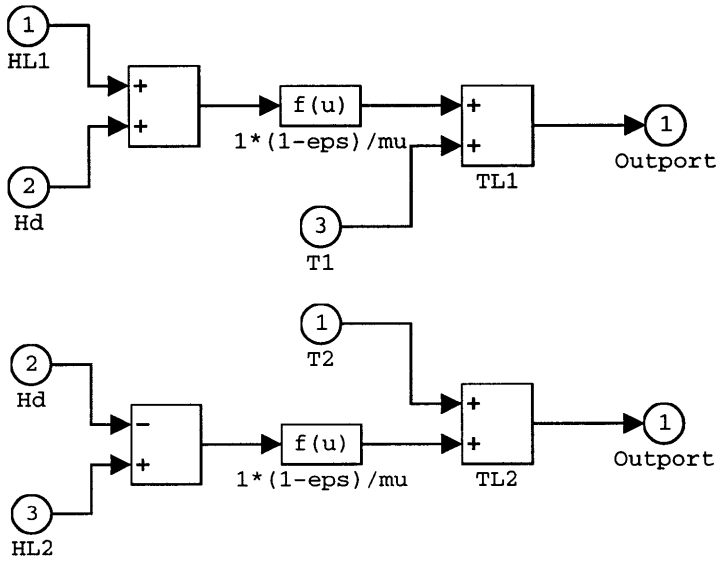

Surface heat fluxes into the ocean: